

NACA TN 3376 8936

0066460



TECH LIBRARY KAFB, NM

NATIONAL ADVISORY COMMITTEE FOR AERONAUTICS

TECHNICAL NOTE 3376

THE EFFECT OF CONTROL STIFFNESS AND FORWARD SPEED ON THE
FLUTTER OF A 1/10-SCALE DYNAMIC MODEL OF A
TWO-BLADE JET-DRIVEN HELICOPTER ROTOR

By George W. Brooks and Maurice A. Sylvester

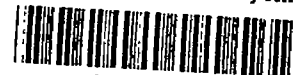
Langley Aeronautical Laboratory
Langley Field, Va.



Washington

April 1955

AFMDC
TECHNICAL LIBRARY
SEL 2811



TECHNICAL NOTE 3376

THE EFFECT OF CONTROL STIFFNESS AND FORWARD SPEED ON THE
FLUTTER OF A 1/10-SCALE DYNAMIC MODEL OF A
TWO-BLADE JET-DRIVEN HELICOPTER ROTOR

By George W. Brooks and Maurice A. Sylvester

SUMMARY

Some experimental studies have been made to determine the general characteristics of rotor-blade flutter under hovering and simulated forward flight conditions by means of flutter tests of the rotor system of a 1/10-scale dynamic model of a two-blade jet-driven helicopter. Tests were made for several configurations to evaluate the effect of variations in the blade-pitch-control stiffness and forward speed on the flutter speed.

The results of the investigation showed that the flutter speed of the model blades was increased as the blade-pitch-control stiffness was increased and indicated that the structural blade modes of primary significance with respect to flutter were the first torsion mode and the flapping mode. The results also showed that the rotor speed at flutter was reduced slightly as the tip-speed ratio was increased from a hovering condition and that the nature of the flutter motion was changed from a sinusoidal oscillation having a distinct frequency to a more random type of oscillation of comparable amplitude but without a well-defined frequency.

INTRODUCTION

As a general rule, helicopter designers are not greatly disturbed by the phenomenon of flutter primarily because rotor blades are generally mass-balanced throughout their length in consideration of other more imminent problems such as undesirable control forces. In addition, the blades of present-day helicopters are less susceptible to flutter because of the relatively low tip speeds. However, these favorable conditions may not exist indefinitely. The introduction of irreversible controls may lead the designer to select blades which are not completely mass-balanced in order to obtain the desired strength with minimum weight. Or in some cases, the internal structure may make it desirable to achieve chordwise mass balance of the blade as a unit by means of concentrated weights

located at selected blade spanwise stations. The use of such design features in conjunction with higher tip speeds may cause flutter of helicopter rotor blades to become a problem.

Experience with the flutter of wings and propellers is of considerable value in the preliminary consideration of helicopter-rotor-blade flutter problems and may indicate the trends to be expected with variations in basic parameters. However, experimental information on the flutter of helicopter rotor blades is desirable to verify these trends and to point out the effects of some of the unique design features and flight conditions of helicopters on their flutter characteristics.

A few years ago, a 1/10-scale dynamic model of a two-blade jet-driven helicopter was constructed primarily to investigate the effects of its unusual design features on various dynamic problems including rotor-blade flutter. The results of the preliminary flutter tests together with a description of the model are given in reference 1. Those tests, made under hovering conditions for values of the model parameters appropriate to a full-scale helicopter having these general characteristics, showed that the model was only marginally safe from the standpoint of flutter. The studies were therefore extended by varying some of the model parameters through a wider range and by including tests under simulated forward-flight conditions in order to obtain flutter data of more general interest.

Tests were made for a wide range of control-system restraint with the model in the hovering condition, and the effects of forward flight were investigated for three different mass distributions, one of which included tabs attached to the trailing edges of the blades. The results of these tests, together with a description of the manner in which the parameters were changed by modification of the model components, are presented.

SYMBOLS

B	bending strain-gage response at flutter, in.
B _r	reference bending strain-gage response, in.
c	blade chord, in.
C _α	torsional-control stiffness, ft-lb/radian
EI	bending stiffness, lb-in. ²

GJ	torsion stiffness, lb-in. ²
$I_{p_{cg}}$	blade polar moment of inertia per unit length about section chordwise center of gravity, slug-ft
I_{tt}	moment of inertia of tab installation about its center-of-gravity location, slug-ft ²
K_{α}	effective Southwell coefficient for first torsion mode
m	mass added to blade, slugs
M	mass of blade, slugs
r	radial distance to blade element, ft
R	blade radius, ft
T	torsional strain-gage response at flutter, in.; restoring torque
T_r	reference torsional strain-gage response, in.
V	simulated forward velocity, ft/sec
μ	tip-speed ratio ($\cos \alpha$ assumed equal to 1), $\frac{V \cos \alpha}{\Omega R}$
μ_f	tip-speed ratio at flutter, $V/\Omega_f R$
Ω	rotor angular velocity, rpm
Ω_f	rotor angular velocity at flutter, rpm
Ω_e	effective rotor angular velocity, rpm
α	rotor angle of attack, radians
ω_f	flutter frequency, cpm
ω_{α}	first torsion frequency at rotational speed Ω , cpm
ω_{α_f}	first torsion frequency at rotational flutter speed Ω_f , cpm
ω_{α_0}	first torsion frequency at $\Omega = 0$, cpm

APPARATUS AND METHODS

Description of Model and Test Configurations

The experimental flutter studies were made with the rotor and pylon suspension system of a 1/10-scale dynamic model of a two-blade, jet-driven helicopter mounted on the tiltable support shown in figure 1. The unconventional design features together with a detailed description of the model components of the design configuration are given in reference 1.

The 13-foot-diameter rotor is powered by a pressure-jet system using a compressed-air power supply. The blades are equipped with two detachable external counterweights to adjust the blade static moment about the quarter chord, and the blade centrifugal forces are transferred to the hub by means of two blade-retention straps. The spanwise distributions of significant blade parameters including blade weight, chordwise center-of-gravity location, mass moment of inertia, and stiffness are given in figures 2 to 5.

The flutter tests were made in two series. The first series consisted of tests with the model in the hovering condition to determine the effect of blade-pitch-control stiffness, and the second series of tests was made under simulated forward-flight conditions (μ up to 0.18) to determine the effects of tip-speed ratio. The blade configurations used in the two series of tests are shown schematically in figures 6(a) and 6(b).

The flutter tests which constitute the first series were made for five configurations of the rotor blades, referred to hereinafter as configurations 1 to 5; these configurations had various control stiffnesses. These changes in control stiffness are shown in figure 6(a) and in table I. The control stiffness is defined as the torque per unit angle of rotation which is required to rotate the blade root about the pitch or feathering axis. In order to provide a convenient means for varying the blade-pitch-control stiffness, the pitch-control arms were disconnected from the swash plate and connected by vertical links to a control beam, the arrangement of which is shown by the sketch of the rotor hub in figure 7. The torsional-control stiffness was varied by using a series of control beams having different stiffnesses. The values of the control stiffness, measured in units of ft-lb/radian, for the configurations tested were 6.45, 19.25, 50.40, 116.0, and 134.2. This control system did not provide for cyclic-pitch variations. The collective-pitch angle was preset to approximately 0° before each test.

The tests which constitute the second series were made for three additional configurations, hereinafter designated as configurations 6, 7, and 8, wherein the control stiffness was held constant at 135.2 and changes were made in the mass distribution of the blades as shown by the blade sketches in figure 6(b). Configuration 6 was essentially the same as

configuration 5 with the outboard counterweight removed. Configuration 7 was identical to configuration 6 except that a small weight was added to the trailing edge of the blade near the tip. For configuration 8, both counterweights were removed from the blades and a fixed trailing-edge tab was installed. Details of the changes in the blade mass distribution for these configurations are given in table II and the details of the tab installation are given in figure 8.

The model tests to determine the effect of blade-pitch-control stiffness on flutter were made with the tiltable support locked in the vertical position. The center of the rotor was located approximately 1 rotor diameter from a wall and about 55 inches above the floor as indicated in the sketch of the rotor support shown in figure 9.

The model tests to evaluate the effect of tip-speed ratio on flutter were made in the return passage of the Langley full-scale tunnel where average velocities up to about 35 ft/sec could be obtained. The maximum random fluctuations in the flow were approximately 120 percent of the average velocity. The rectangular cross section of the passage at the test area is approximately 50 feet wide and 65 feet high. The rotor center was located 85.5 inches above the floor (see fig. 9) and midway between the tunnel walls. During these tests, the upper section of the rotor support was tilted forward (into the wind) approximately 3.1° so that it corresponded to the normal shaft configuration of the prototype in cruising flight.

Instrumentation

The instrumentation of the model consisted of a rotor-speed tachometer, a one-per-revolution rotor-speed timer, a tunnel velocity indicator, and strain-gage installations on the blades. The outputs from the rotor-speed timer, tunnel velocity indicator, and strain gages were recorded on oscillograph records. A sample record is shown in figure 10.

The rotor-speed tachometer consisted of a small multipole generator, the armature of which was attached to the rotor hub by means of a flexible coupling. The generator output was fed into a commercial device for measuring frequencies which showed the rotor speed directly on a series of dials.

The one-per-revolution rotor-speed timer consisted of a spring-loaded brush-contact arrangement which effected a break in an oscillograph galvanometer circuit once each revolution of the rotor. Time intervals were obtained from a 60-cycle timing trace on the record.

The tunnel velocity indicator consisted of a small sphere mounted on a strain-gage cantilever beam which was located on a rigid support at the same height as the rotor above the floor and one radius upstream and one

diameter to the starboard of the rotor center. The output of the gages, which depended on the drag of the sphere, was recorded and converted to the tunnel velocity by means of an established calibration factor.

Strain gages were mounted on the exterior surfaces of the blades in the vicinity of the quarter chord at station 47 (0.6 blade radius) to indicate the frequencies and amplitudes of the bending and torsion blade deformations.

Testing Technique

The flutter tests in the hovering condition were made by gradually increasing the rotor speed until flutter occurred. As soon as possible after the blades began to flutter, the air supply to the rotor was reduced. A similar procedure was followed, in the investigation of the effect of tip-speed ratio on flutter, for a series of discrete tunnel velocities ranging from 0 to a maximum velocity of about 35 ft/sec (μ up to 0.18).

RESULTS AND DISCUSSION

Observations during the flutter tests indicated that, in some cases, the blades tended to diverge or go out of track before flutter was encountered; that is, at a certain rotor speed the tip-path planes of the two individual blades ceased to be coincident and one blade tracked above its normal plane of rotation and the other below. The amount of out-of-track then increased rapidly with increased rotor speeds. When some of the flutter data were obtained, particularly those for the lower values of pitch-control stiffness, it was often necessary to tolerate amounts of out-of-track equal to as much as 20 percent of the blade radius. When the blades commenced to flutter, however, they appeared to oscillate about the normal plane of rotation. The tendency of the blades to diverge was more pronounced during the hovering tests than during the forward-flight flutter tests.

An examination of the records showed that, after the flutter commenced and after the power to the rotor had been cut off, the flutter of the model blades usually continued to a rotor speed well below that at which flutter was initially encountered. In the hovering condition, the rotor speed at which flutter stopped was in some cases as much as 25 percent below the rotor speed at which flutter started and changes in the flutter mode and frequency were often noted as the flutter continued to the lower rotor speed. During the forward-flight tests, the differences in the rotor speeds at the beginning and end of flutter were generally less than 10 percent. The flutter data presented in this paper correspond to the points where flutter commenced.

The pertinent model parameters and the flutter test results are given in tables I to III and in figures 10 to 16 and are discussed in the subsequent sections.

Effect of Blade-Pitch-Control Stiffness

Tests have shown that the flutter speed and associated flutter frequency of the classical bending-torsion type of flutter of most aerodynamic structures such as wings, propellers, and rotor blades are strongly dependent on the torsional stiffness which is characterized by the first torsional frequency. (The first torsional frequency referred to herein is the frequency of the first coupled mode which is predominantly torsion. Since the elastic axis and the chordwise center-of-gravity axis of the blade are nearly coincident, the amount of bending in this coupled mode is small.) The torsional frequency ω_α for a rotor blade at any rotor speed Ω is given approximately by an equation of the general form

$$\omega_\alpha^2 = \omega_{\alpha_0}^2 + K_\alpha \Omega^2$$

where ω_{α_0} is the torsional frequency at $\Omega = 0$ and K_α is an effective Southwell coefficient for blade torsion which depends on the root-control system as well as on the blade flexibility. Experimental and theoretical studies were made to determine the appropriate values for K_α for each value of C_α , and the results of these studies are discussed in the appendix.

The variation of torsional frequency with rotor speed, for each blade-pitch-control-stiffness configuration, is shown by the dashed lines in figure 11 together with the flutter boundary which shows the effect of changes in blade-pitch-control stiffness on the rotor speed at flutter. Curves of limiting frequencies which correspond to values of blade-pitch-control stiffness of zero and infinity are also shown. The data presented in figure 11 show that flutter was obtained over the entire range of blade-pitch-control stiffnesses tested at rotor speeds above the normal operating speed of the model. The flutter speed is reduced approximately 22 percent as the control stiffness is varied from 135.2 ft-lb/radian to 19.25 ft-lb/radian. It appears that a minimum value of the flutter speed occurs at $C_\alpha \approx 19.25$ since there is a slight increase in the flutter speed as the control stiffness is further reduced to 6.45 ft-lb/radian.

For the model tested, there is a large increase in the blade torsional frequencies with rotor speed due largely to the torsional restoring moment which results when centrifugal forces act on the blade-retention straps,

The results shown in figure 11, however, should be generally applicable to a similar blade mounted in a more conventional manner (without straps) and having a higher torsional control stiffness C_α to give corresponding torsional frequencies at flutter.

Motion pictures and visual observations of the flutter showed that the motion of the various blade elements during flutter consisted of a combination of translation in the flapping plane and torsion and that a large part of the translation of the blade elements was due to blade flapping. The oscillograph records of the flutter showed that some elastic bending of the blade was also present; however, the structural modes which primarily affect the flutter characteristics of the blades are the first torsional mode and the flapping mode. This conclusion is emphasized in figure 12 where the significant blade frequencies are shown as a function of the rotor speed at flutter. The increase in the frequencies of the flapping and first bending modes with rotor speed at flutter are due only to the effects of centrifugal forces, whereas the corresponding increase in the frequency of the first torsion mode is due to the combined effects of centrifugal force and changes in the blade-pitch-control stiffness. The data in figure 12 show that, for all configurations studied, the flutter frequency is approximately midway between the first torsion or first bending frequency and the flapping frequency. The results of flutter tests of wings involving coupling of primary bending and torsion modes show that the flutter frequency usually has a value which is between the frequencies of the modes involved. Inasmuch as it was established by observations of the flutter motion of the blades that substantial blade torsion was present during flutter, and inasmuch as the data presented in figure 11 show a substantial variation in flutter speed with torsional frequency, it is concluded that the blade modes of primary significance are the flapping mode and first torsion mode.

The loops in the curves for the first torsional frequency and the flutter frequency which are shown at the lower flutter speeds in figure 12 are a reflection of the fact that the flutter data presented in figure 11 show an increase in flutter speed as the torsional frequency is reduced below about 800 cpm. However, the data show that, even though the flutter speed is increased slightly for the lowest value of the control stiffness tested, the flutter frequency is reduced approximately in proportion to the blade torsional frequency.

Effect of Tip-Speed Ratio

The effect of tip-speed ratio on the rotor speed at flutter for the three configurations tested is shown in figure 13. These data show that the rotor speed at flutter is slightly lower at the higher tip-speed ratios than it is at the lower tip-speed ratios. For configurations 6 and 8 the

reduction in flutter speed occurred largely between $\mu = 0$ and $\mu = 0.10$ whereas for configuration 7 the flutter speed was increased for this range of tip-speed ratio and decreased for tip-speed ratios of 0.10 to 0.18.

Since there are large changes in velocity over the blades as the blades rotate during forward flight, it is interesting to examine a plot of the actual velocity over the blade tip at flutter to determine the extent to which these fluctuations in velocity may contribute to the reduced rotor speed at flutter. Figure 14 shows the rotor-tip speed at flutter, due to blade rotation, and the corresponding tip speeds of the advancing and retreating blades as a function of the tip-speed ratio for configuration 6. At a given value of μ , the blade-tip speed at flutter would actually be fluctuating between the maximum and minimum tip-speed values shown in figure 14. This fluctuation indicates that the tip speed at flutter for the forward-flight tests exceeded the tip speed at flutter for the hovering tests ($\mu = 0$) for a part of each revolution of the blade. Thus, for this configuration, flutter did not occur in the forward-flight condition when the velocity of the advancing blade reached the flutter speed of the blade in the hovering condition.

In addition to affecting the flutter speed slightly, forward flight also caused noticeable changes in other model flutter characteristics as shown in figure 10 by the comparison of flutter records obtained during hovering- and forward-flight conditions. The flutter motions at $\mu = 0$ were characterized by sinusoidal oscillations with well-defined frequencies whereas at forward speeds the flutter oscillations were very irregular and the flutter frequencies could be determined only approximately. For this reason only the flutter frequencies for the tests in the hovering condition are listed in table II.

In addition to showing the effect of tip-speed ratio on rotor-blade flutter, the results presented in table II and figure 13 also show that the flutter speed is reduced by the addition of a concentrated weight to the blade near the tip and rearward of the chordwise center-of-gravity location. The results further show that the installation of fixed tabs to the blades at the trailing edge near the tip results in a slightly higher flutter speed and somewhat lower flutter stresses at station 47 than would be expected from the addition of concentrated weights having the same mass and inertia characteristics.

Effect of Flutter on Blade Stresses

The phenomenon of flutter is of interest primarily as a result of the large stresses which the fluttering blades impose on themselves and other components of the helicopter structure. During the present investigation, the blade strains encountered during flutter were measured at station 47 and are proportional to the trace amplitudes listed in table II

where B is the amplitude of the bending-trace deflection and T is the amplitude of the torsion-trace deflection. For the sake of comparison, the bending- and torsion-trace amplitudes measured during a transition from hovering to forward flight at the normal rotor speed of 283 revolutions per minute are given in figure 15 for configuration 6. Table III presents a tabulation of these reference trace amplitudes (designated by subscript r) and the trace amplitudes measured during flutter as well as the ratios B/B_r and T/T_r . These ratios, which are equivalent to the ratios of blade stresses, are plotted as a function of the tip-speed ratio in figure 16.

Figure 16 shows that the stresses measured during flutter are significantly higher than those measured during normal operation. This condition is particularly true in the case of blade torsion and at tip-speed ratios near zero. The large decrease in the ratio of the stresses between $\mu = 0$ and $\mu = 0.09$, as well as the increase in the stress ratio at the higher values of μ , may be attributed largely to the variation in the reference stresses with tip-speed ratio as shown by the curves of figure 15. The magnitudes of the flutter stresses were approximately the same throughout the range of tip-speed ratios studied.

CONCLUSIONS

As a result of the investigation of the rotor-blade flutter characteristics of a 1/10-scale dynamic model of a two-blade jet-driven helicopter, the following conclusions are presented:

1. The effect of increasing the torsional frequency of the blades by increasing the stiffness of the blade-pitch-control mechanisms was to increase the flutter speed and flutter frequency.
2. The flapping mode and the first torsion mode appear to be of primary significance in that the flutter mode and frequency appear to be chiefly the result of the coupling of these two modes.
3. The effect of forward velocity was to decrease the rotor speed at flutter slightly; however, the resultant tip speed of the advancing blade at flutter increased with tip-speed ratio.
4. As the tip-speed ratio is increased from zero, the flutter motions change from a well-defined sinusoidal oscillation having a distinct frequency to a more random type of oscillation of comparable amplitude but without a well-defined frequency.
5. The blade stresses encountered at station 47 (0.6 blade radius) during flutter were much higher than those encountered during normal flight at similar tip-speed ratios and under similar atmospheric conditions.

This result was most pronounced under hovering conditions where the stresses under normal flight conditions are very low and the flutter stresses very high.

Langley Aeronautical Laboratory,
National Advisory Committee for Aeronautics,
Langley Field, Va., December 7, 1954.

APPENDIX

DETERMINATION OF ω_{α_0} AND EFFECTIVE SOUTHWELL COEFFICIENT

FOR THE VARIATION OF THE FIRST TORSIONAL FREQUENCY

WITH ROTOR SPEED FOR VARIOUS CONTROL STIFFNESSES

The effect of centrifugal force on the natural frequency of the first torsional mode of the blade is to increase the natural frequency approximately as follows:

$$\omega_{\alpha}^2 = \omega_{\alpha_0}^2 + K_{\alpha} \Omega^2$$

where ω_{α} is the torsional frequency at rotor speed Ω and ω_{α_0} is the torsional frequency when $\Omega = 0$. The coefficient K_{α} is commonly referred to as the Southwell coefficient for torsion.

Determination of ω_{α_0}

In general, ω_{α_0} can be calculated from spanwise distributions of the mass moment of inertia about the torsion axis and the torsional stiffness GJ of the blade or it can be obtained experimentally. In this particular case, ω_{α_0} was obtained experimentally by mounting the blades on the hub in the test configuration. Each blade was supported on a single elastic shock cord at the spanwise location of the node of the first elastic bending mode. The tips of the blades were then deflected in torsion and the frequency was obtained from oscillograph records of blade strain-gage responses following instantaneous removal of the applied torque at the blade tip. The same procedure was followed for each change in blade-pitch-control stiffness.

Determination of K_{α}

Effect of tension on blade stiffness.—In general, the influence of centrifugal forces on the torsional frequency is due to two separate effects. The first of these is the stiffening effect due to the tendency of centrifugal forces to reduce the amount of blade twist by straightening the fibers

of the blade. This effect is discussed in some detail in reference 2 where the restoring torque T at any spanwise station of the blade is given as:

$$T = \frac{F I_{cg}}{A} \phi$$

where

F	centrifugal tensile force in the blade
A	stressed area of the cross-section
I_{cg}	area moment of inertia of the stressed area of the cross section about the centroid of the stressed area
ϕ	blade twist per unit length of span

Since the centrifugal force F is proportional to Ω^2 , this effect can be treated as a part of the Southwell coefficient. Calculations made for the present blades indicate a value of K_α of 0.17.

Effect of chordwise components of centrifugal forces.- The second contribution of centrifugal forces toward the increase in torsional frequency with rotor speed arises from the fact that the chordwise components of the centrifugal forces acting on any element of a blade act in such a manner as to reduce the angle between the blade element and the plane normal to the shaft. This effect is discussed in some detail in reference 3 and leads to a value of K_α of approximately 1 for rotor blades.

Bifilar effect.- In addition to the effects previously discussed, the natural torsional frequency of the present design is also subject to an additional effect of centrifugal force by virtue of the fact that attachment of the blade to the hub by means of the blade-retention straps is essentially a bifilar suspension. The restoring torque in this case is a function of the blade pitch angle, the distance between the straps, the length of the straps, and the centrifugal force at the point of strap attachment to the blade flanges. In the present case, if the blade is assumed to rotate about the feathering or pitch bearing as a rigid body, calculations yield a Southwell coefficient of 4.24.

Effective Southwell coefficient.- The effective Southwell coefficient is obtained by a combination of the three effects previously discussed and varies with the blade-pitch-control stiffness. This variation is explained as follows: If the blade-pitch-control stiffness is zero, the natural frequency of the bifilar-suspension system is substantially below the first natural frequency of the blade and only negligible blade deformations occur when the blade vibrates in torsion about the blade-pitch bearing.

In this case, the effective value of K_α is obtained by adding the bifilar value of the Southwell coefficient of 4.24 to the contribution of the chordwise components of centrifugal force which has a value of 1. The effective value of 5.24 is shown in figure 17.

At the other extreme, as the blade-pitch-control stiffness becomes very large, the bifilar effect diminishes and it approaches zero when the blade-root attachment is fixed. In the latter case, the Southwell coefficient approaches the value of 1.17 which represents the combined effect of the spanwise and chordwise components of centrifugal forces acting on the blade elements. In this case the value of 1.17 corresponds to a frequency ω_{α_0} of 1,440 cpm as shown in figure 17. At all values of ω_{α_0} less than 1,440 cpm and greater than 0, the effective value of K_α would be greater than 1.17 and less than 5.24.

In an effort to determine the effective values of K_α for the control stiffnesses employed in the model tests, the rotor hub was mounted on a rigid support and the blades were allowed to hang vertically. For each blade-pitch-control-stiffness configuration, the blade-retention straps were loaded in tension by applying various loads to the blade-root attachment (fig. 7) in a manner which would simulate centrifugal forces. The natural frequencies of the blades in this condition were measured for each configuration and are plotted in figure 18 as a function of the effective rotor speed for each control stiffness. The effective rotor speed is defined as the speed at which the centrifugal force on the retention straps would be equal to the applied load. The theoretical frequencies obtained when the blade-pitch-control stiffness C_α approaches zero and infinity are also shown. Curves were faired through the experimental data points and calculations were made to determine the Southwell coefficient associated with each curve. A value of 1 was then added to the measured value to account for chordwise centrifugal-force effects which were not simulated and the resulting coefficients were plotted in figure 17. The curve faired through the data points of figure 17 is assumed to give the approximate effective value of K_α for all values of ω_{α_0} . These values of K_α are used to determine the torsional frequency of the blades used in the presentation of the flutter data in figure 11.

Effect of control stiffness on torsional frequencies ω_{α_0} . - A rather interesting study of the manner in which the flexibility of the blade and the blade-pitch-control stiffness combine to control the torsional frequency is afforded by figure 19 where $\omega_{\alpha_0}^2$ is plotted as a function of C_α . Boundaries are presented for the blade pitching as a rigid body

about the pitch bearing and for the blade clamped at the blade-root attachment flange and twisting as a cantilever beam. For the model design value of $C_\alpha = 87.8$, the curve of measured frequencies shows that the natural mode of torsional vibration consists of a combination of blade pitching as a rigid body and blade twisting as a cantilever.

REFERENCES

1. Brooks, George W., and Sylvester, Maurice A.: Description and Investigation of a Dynamic Model of the XH-17 Two-Blade Jet-Driven Helicopter. NACA RM L50I21, 1951.
2. Biot, M. A.: Increase of Torsional Stiffness of a Prismatical Bar Due to Axial Tension. Jour. Appl. Phys., vol. 10, no. 12, Dec. 1939, pp. 860-864.
3. Sterne, L. H. G.: The Structural Aspects of Propeller Design. Rep. No. Structures 5, British R.A.E., July 1947.

TABLE I.- RESULTS OF FLUTTER TESTS UNDER SIMULATED
HOVERING CONDITIONS

[Basic blade configuration; both counterweights attached]

Configuration	C_{α} , ft-lb/radian	ω_{α_0} , cpm	K_{α}	Ω_f , rpm	ω_{α_f} , cpm	ω_f , cpm	$\frac{\omega_f}{\omega_{\alpha_f}}$
1	6.45	337	4.71	{ 308 310 321 333	{ 749 752 774 798	{ 524 524 554 565	{ 0.700 .698 .716 .708
2	19.25	533	4.32	{ 305 306 313 313 343	{ 828 830 841 841 890	{ 600 600 570 579 630	{ .724 .723 .678 .689 .707
3	50.40	823	3.51	{ 336 346 353 353	{ 1,036 1,046 1,056 1,056	{ 692 697 720 720	{ .668 .666 .682 .682
4	116.0	1,104	2.50	{ 375 379 379 379 379	{ 1,254 1,256 1,256 1,256 1,256	{ 744 735 760 760 765	{ .593 .585 .606 .606 .609
5	135.2	1,160	2.28	{ 391 400 400 400 400	{ 1,302 1,309 1,309 1,309 1,309	{ 788 817 825 831 837	{ .605 .624 .631 .635 .639

TABLE II.- RESULTS OF FLUTTER TESTS UNDER SIMULATED

FORWARD-FLIGHT CONDITIONS

(a) Inboard counterweight attached; outboard counterweight removed; $n_{b0} = 1,248$ cpm; configuration 6

Test	μ	Flutter speed, rpm	Flutter frequency, cpm	B, in. (a)	T, in. (a)
1	0	360	13.3	1.13	2.72
2	0	379	13.3	1.95	3.85
3	0	380	13.3	1.65	3.52
4	.067	346	-----	1.15	2.47
5	.076	353	-----	1.46	2.50
6	.077	350	-----	1.40	3.16
7	.077	357	-----	1.20	2.35
8	.080	350	-----	1.40	2.99
9	.083	350	-----	1.20	2.50
10	.096	353	-----	1.75	3.35
11	.112	343	-----	1.74	2.95
12	.119	340	-----	1.73	3.20
13	.121	348	-----	1.38	2.60
14	.142	340	-----	1.75	2.90

(b) Inboard counterweight attached; outboard counterweight removed; $1/8$ lb ($m/M = 0.025$) concentrated weight added to blade at station 67 at 96.2 percent chord; $n_{b0} = 1,209$ cpm; configuration 7

Test	μ	Flutter speed, rpm	Flutter frequency, cpm	B, in. (a)	T, in. (a)
15	0	310	12.2	0.86	2.66
16	0	305	12.1	.68	2.10
17	0	295	11.7	.84	1.86
18	.068	305	-----	1.20	1.40
19	.076	313	-----	.78	1.40
20	.088	319	-----	1.58	2.40
21	.090	310	-----	1.10	1.55
22	.102	310	-----	2.00	3.20
23	.103	310	-----	.70	1.25
24	.132	293	-----	1.30	1.28
25	.135	297	-----	.96	1.28
26	.177	285	-----	1.76	2.78
27	.183	285	-----	1.10	1.30

(c) Both counterweights removed; 4- by 10-inch tab installed (tab installation described in fig. 4); configuration 8

Test	μ	Flutter speed, rpm	Flutter frequency, cpm	B, in. (a)	T, in. (a)
28	0	316	11.0	0.76	2.50
29	0	322	11.1	.94	2.64
30	.098	293	-----	.58	1.10
31	.098	293	-----	.64	1.04
32	.101	286	-----	.68	1.00
33	.128	300	-----	.80	1.38
34	.128	300	-----	.97	.66
35	.140	285	-----	.66	1.06
36	.166	290	-----	1.18	1.30
37	.174	286	-----	1.14	1.20
38	.176	283	-----	1.00	1.36

^aOscillograph trace deflection (proportional to strain) which is defined in section entitled "Effect of Flutter on Blade Stresses."

TABLE III.- COMPARISON OF BLADE BENDING AND TORSION STRAIN-
GAGE TRACE DEFLECTIONS DURING FLUTTER WITH TRACE DEFLECTIONS
DURING NORMAL OPERATION AT DESIGN ROTOR SPEED OF 283 RPM
[Configuration 6]

Test	μ	B, in.	B_r , in.	B/B_r	T, in.	T_r , in.	T/T_r
1	0	1.13	0.19	5.95	2.72	0.05	54.30
2	0	1.95	.19	10.30	3.85	.05	76.90
3	0	1.65	.19	8.68	3.52	.05	70.40
4	.067	1.15	.72	1.60	2.47	.44	5.61
5	.076	1.46	.78	1.87	2.50	.50	5.00
6	.077	1.40	.78	1.79	3.16	.50	6.32
7	.077	1.20	.78	1.54	2.35	.50	4.70
8	.080	1.40	.79	1.77	2.99	.51	5.86
9	.083	1.20	.81	1.48	2.50	.53	4.72
10	.096	1.75	.84	2.09	3.35	.57	5.88
11	.112	1.74	.87	2.00	2.94	.62	4.74
12	.119	1.73	.85	2.04	3.20	.63	5.08
13	.121	1.38	.80	1.72	2.60	.60	4.33
14	.142	1.75	.59	2.97	2.90	.38	7.63

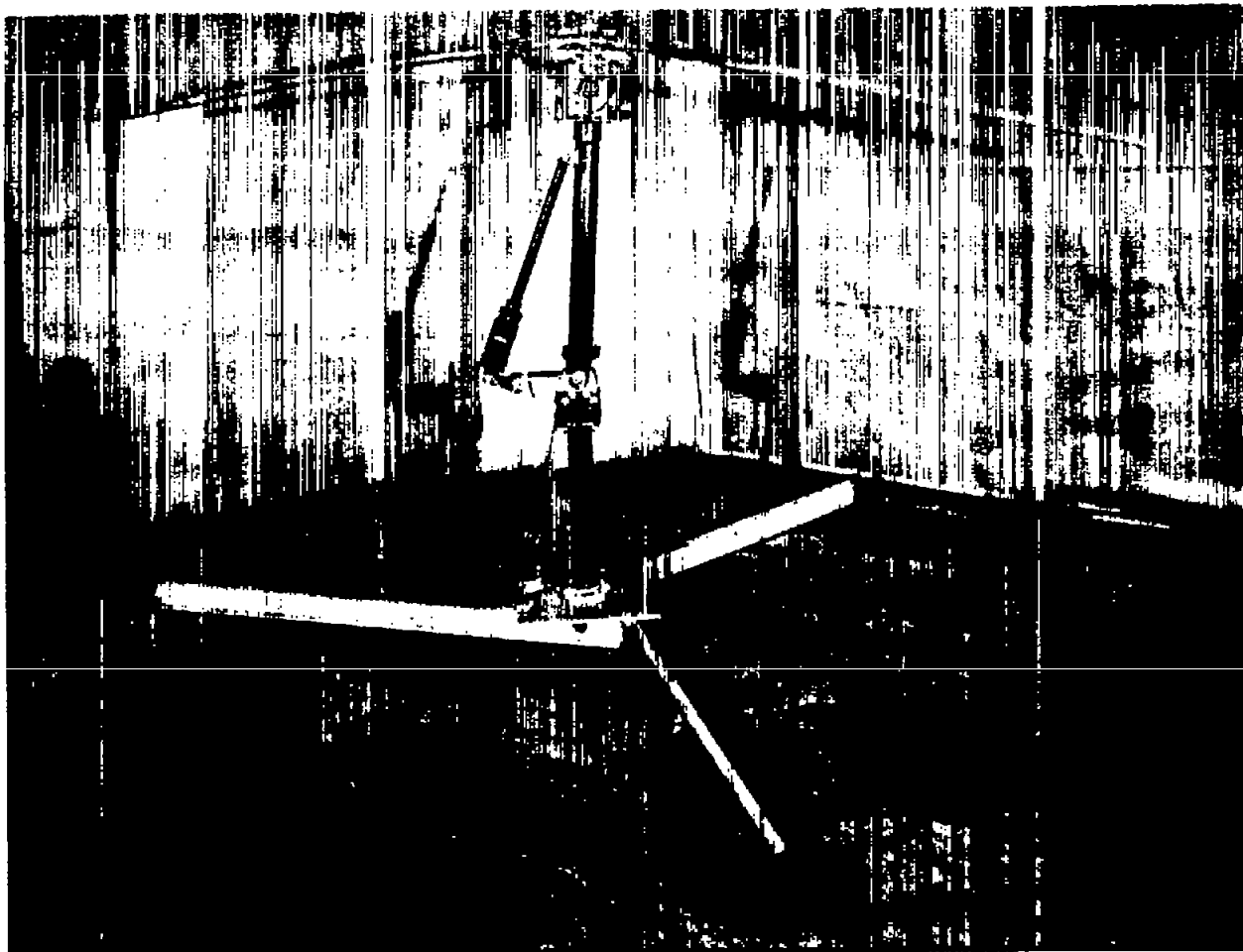


Figure 1.- Rotor mounted on test stand. L-85028

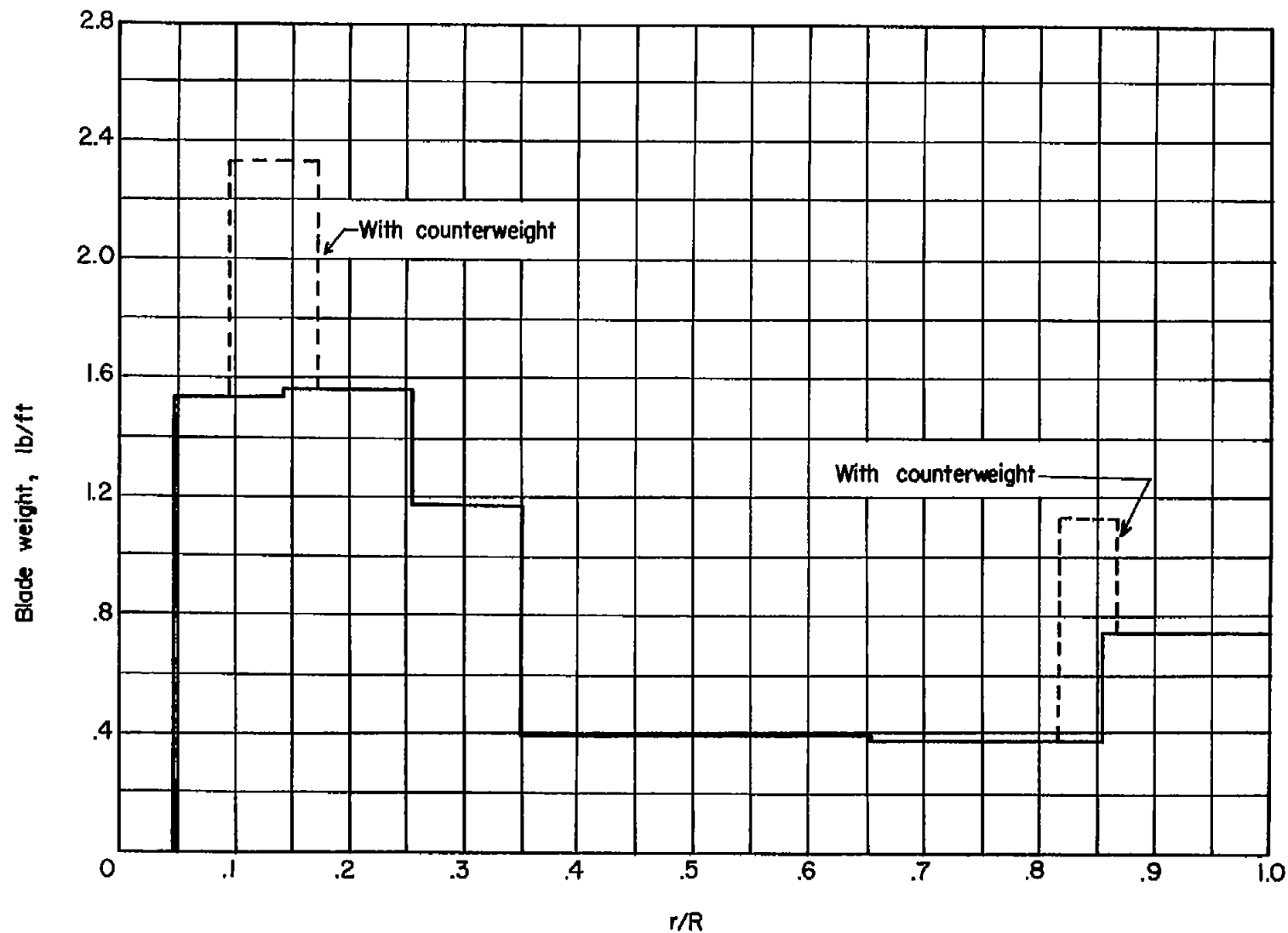


Figure 2.- Spanwise variation of blade weight distribution.

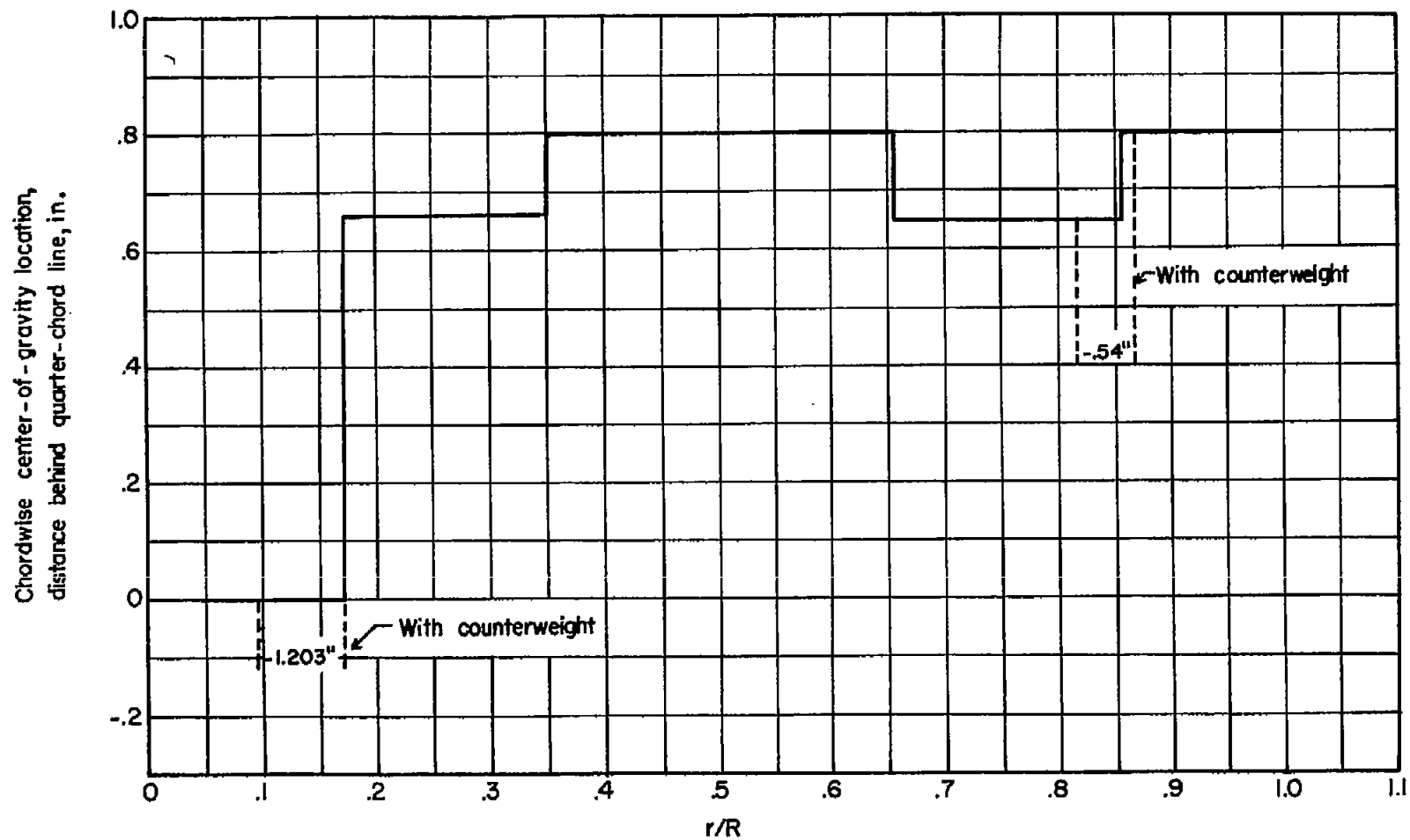


Figure 3.- Spanwise variation of blade chordwise center-of-gravity location.

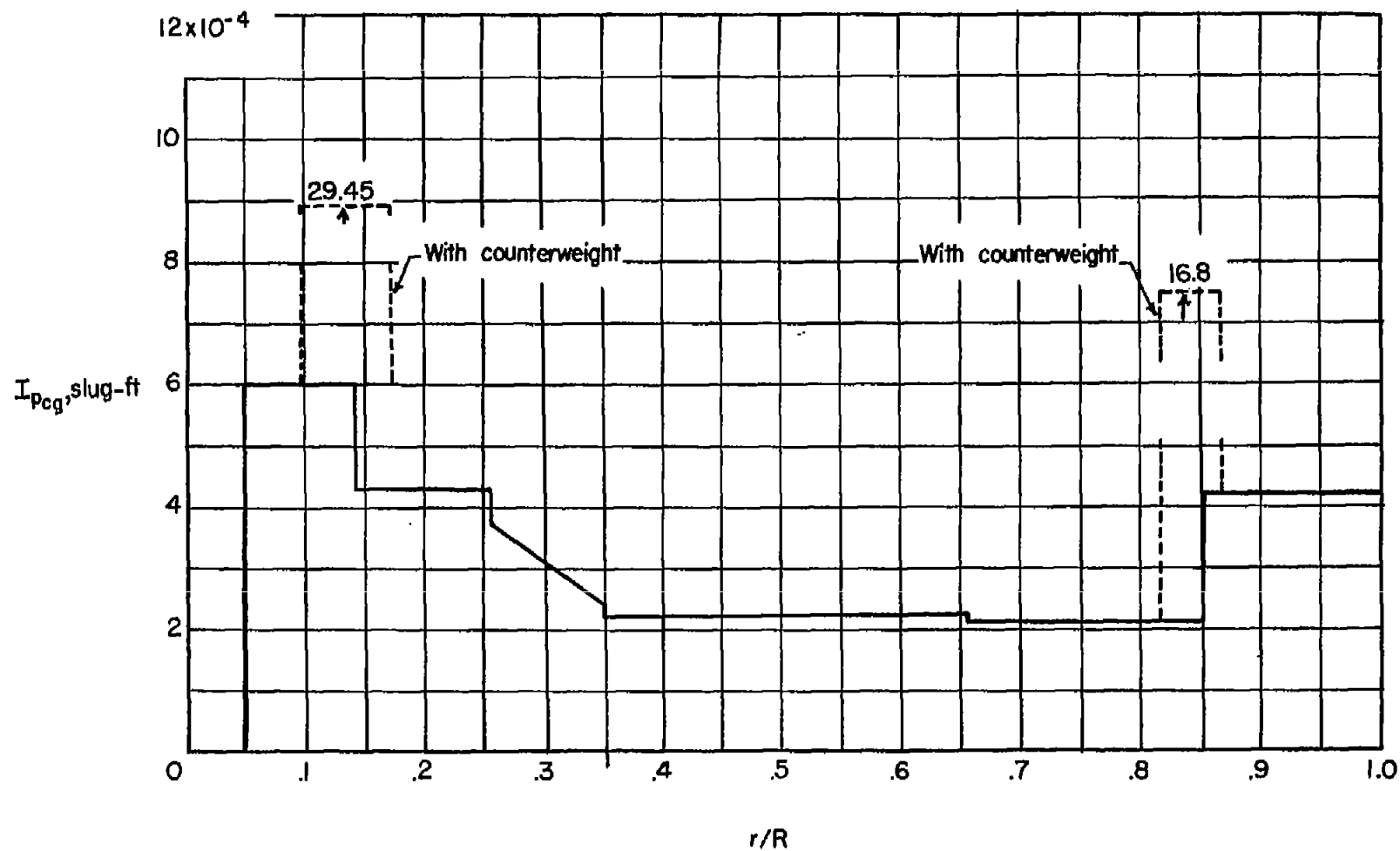


Figure 4.- Spanwise variation of blade mass moment of inertia about section center of gravity.

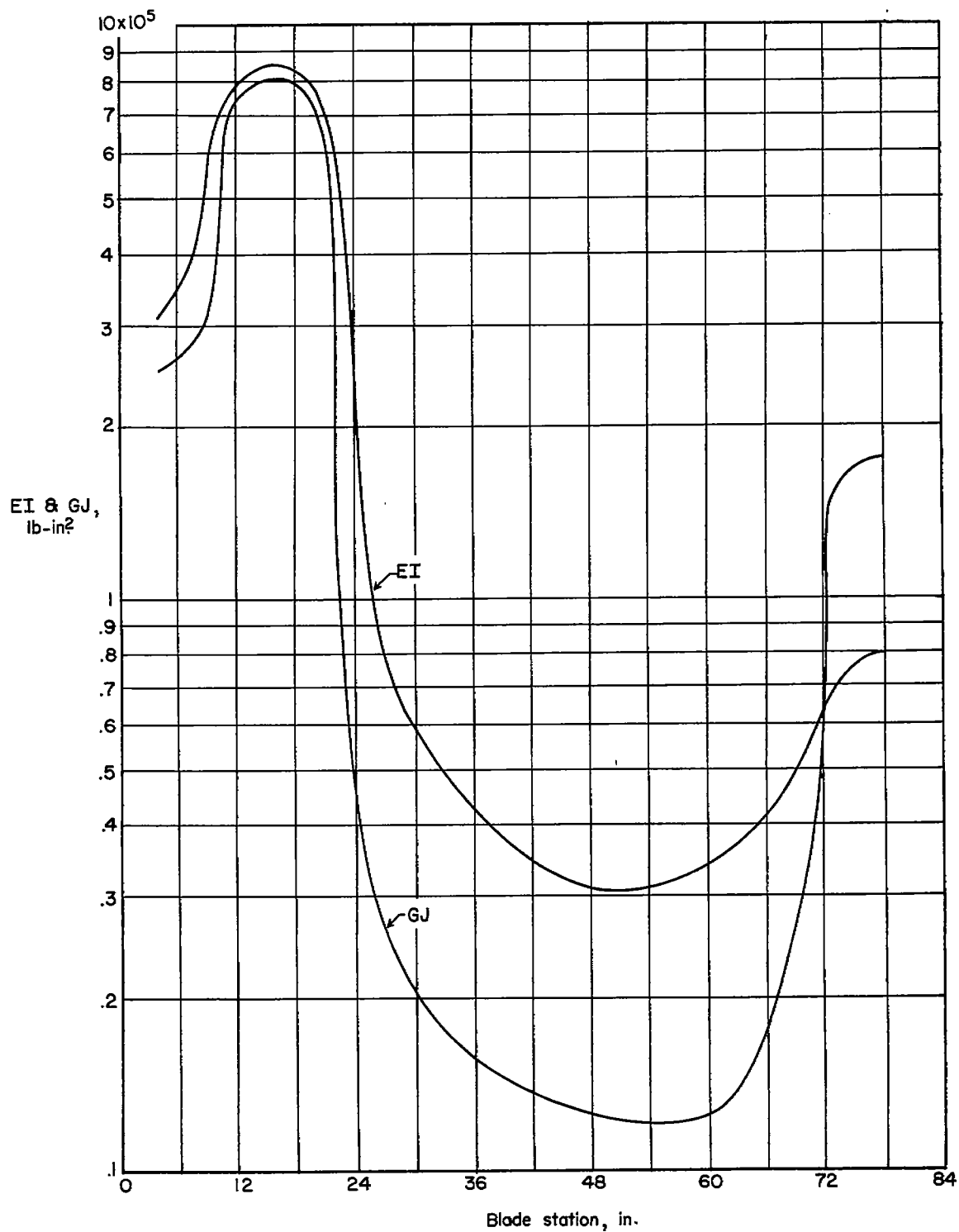
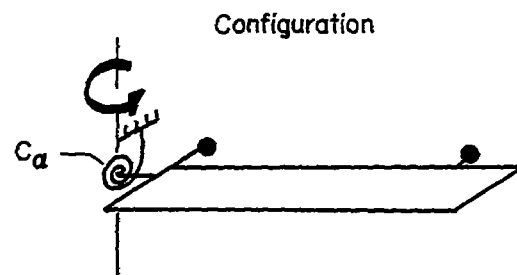


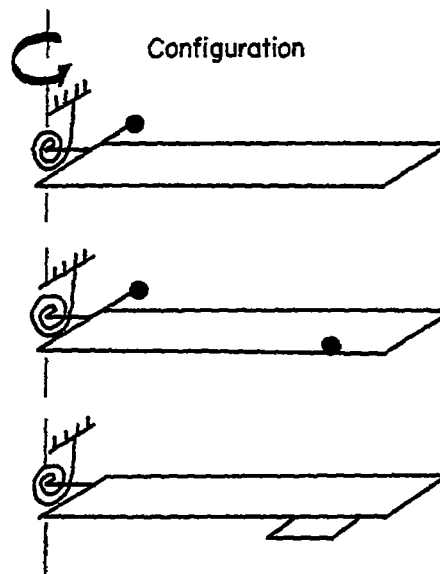
Figure 5.- Spanwise variation of blade bending and torsional stiffness.

Configuration	C_a , ft-lb/radian
1	6.45
2	19.25
3	50.40
4	116.00
5	135.20



(a) Blade configuration used to study effect of control-system stiffness.

Configuration	C_a , ft-lb/radian
6	135.20
7	135.20
8	135.20



(b) Blade configurations used to study effect of tip-speed ratio.

Figure 6.- Schematic drawing of blade configurations.

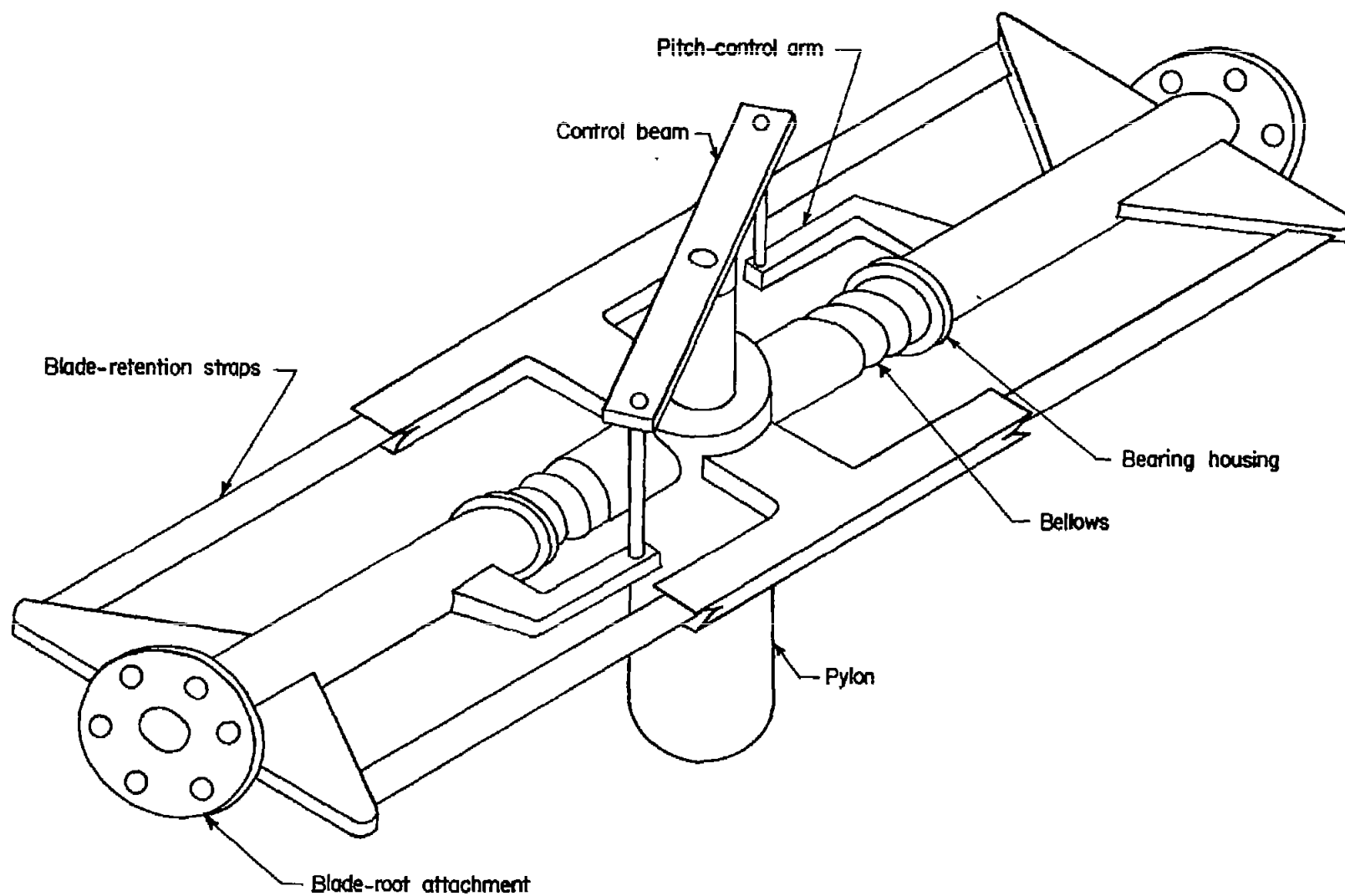


Figure 7.- Schematic drawing of rotor hub showing blade-retention straps and control-beam installation.

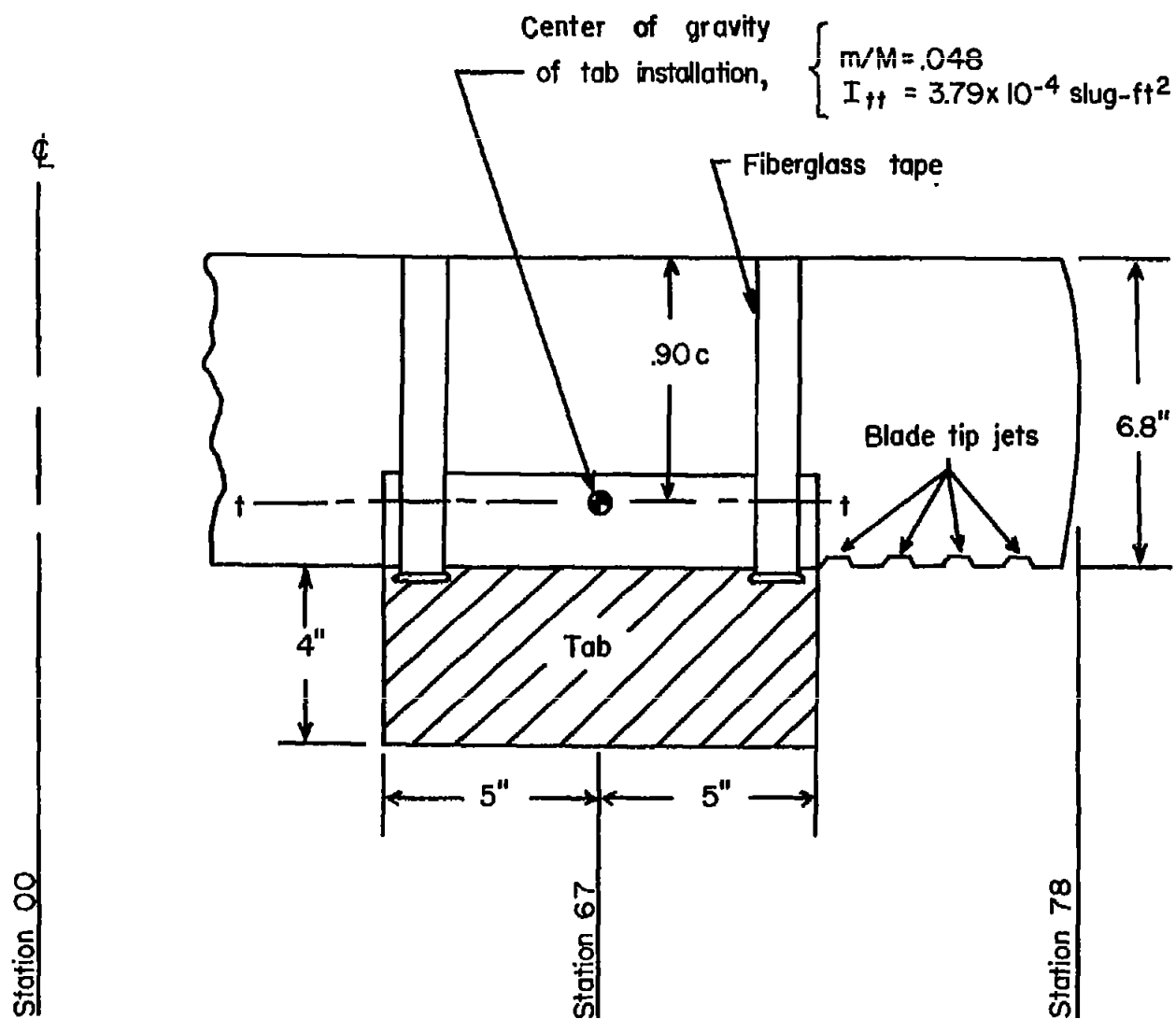


Figure 8.- Blade tab installation.

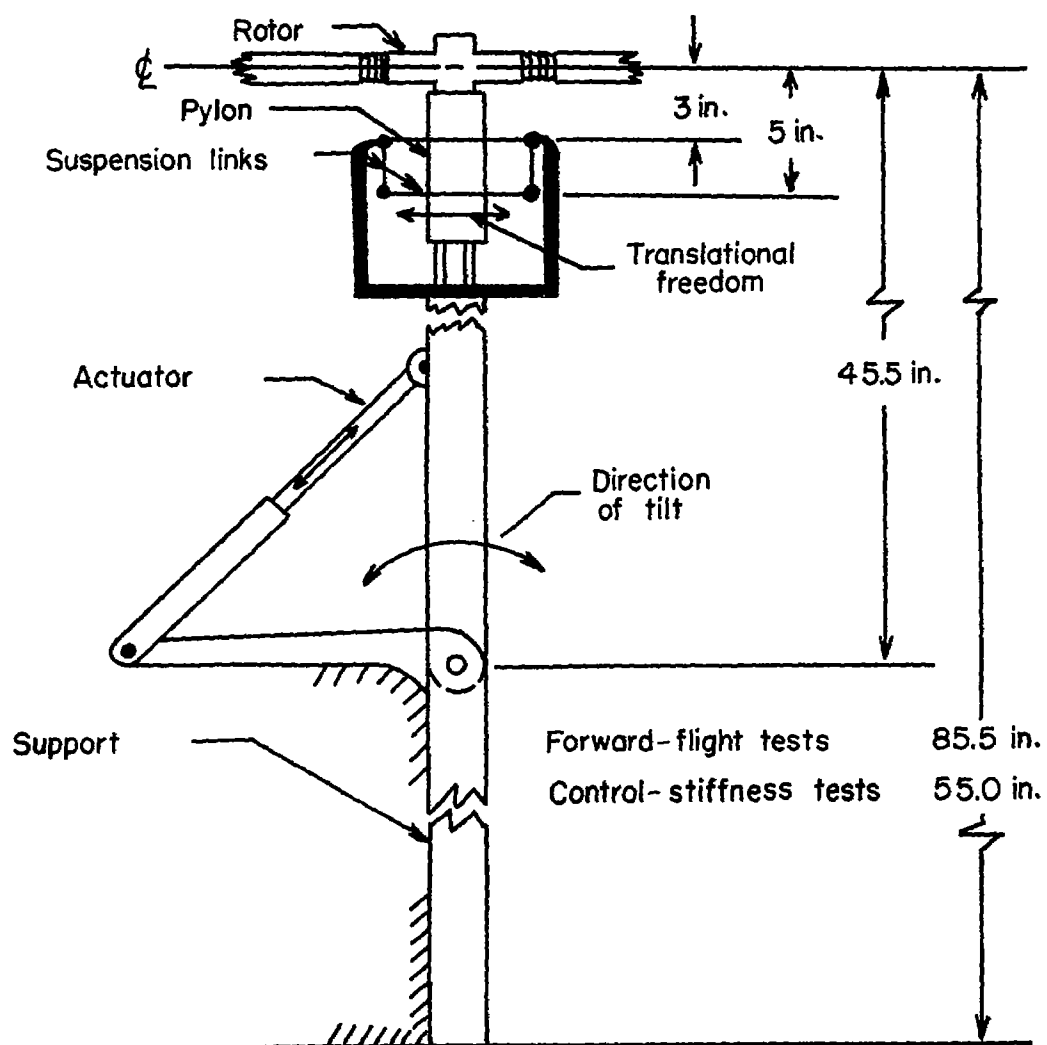


Figure 9.- Dimensional sketch of rotor support.

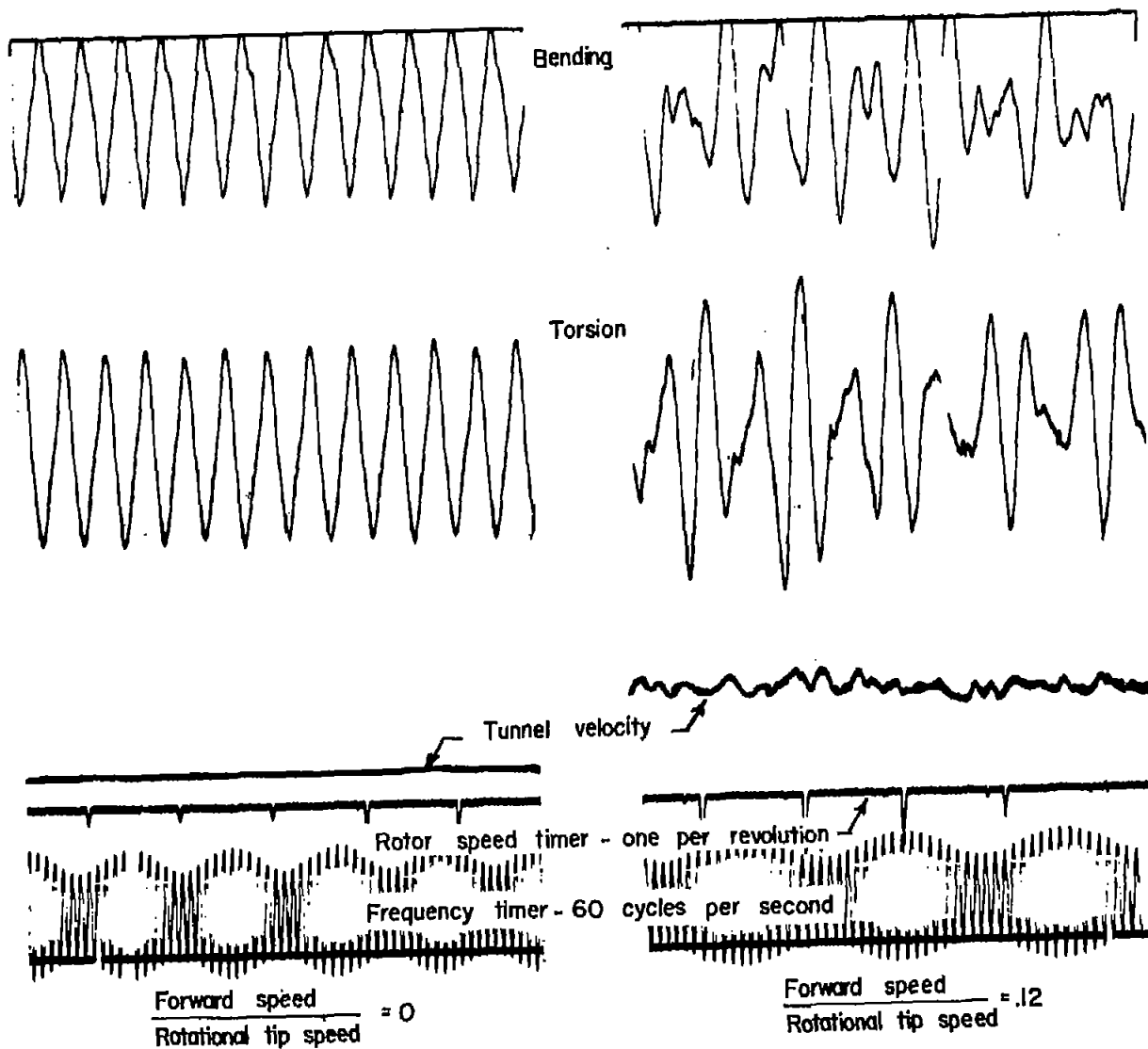


Figure 10.- Sample of flutter records.

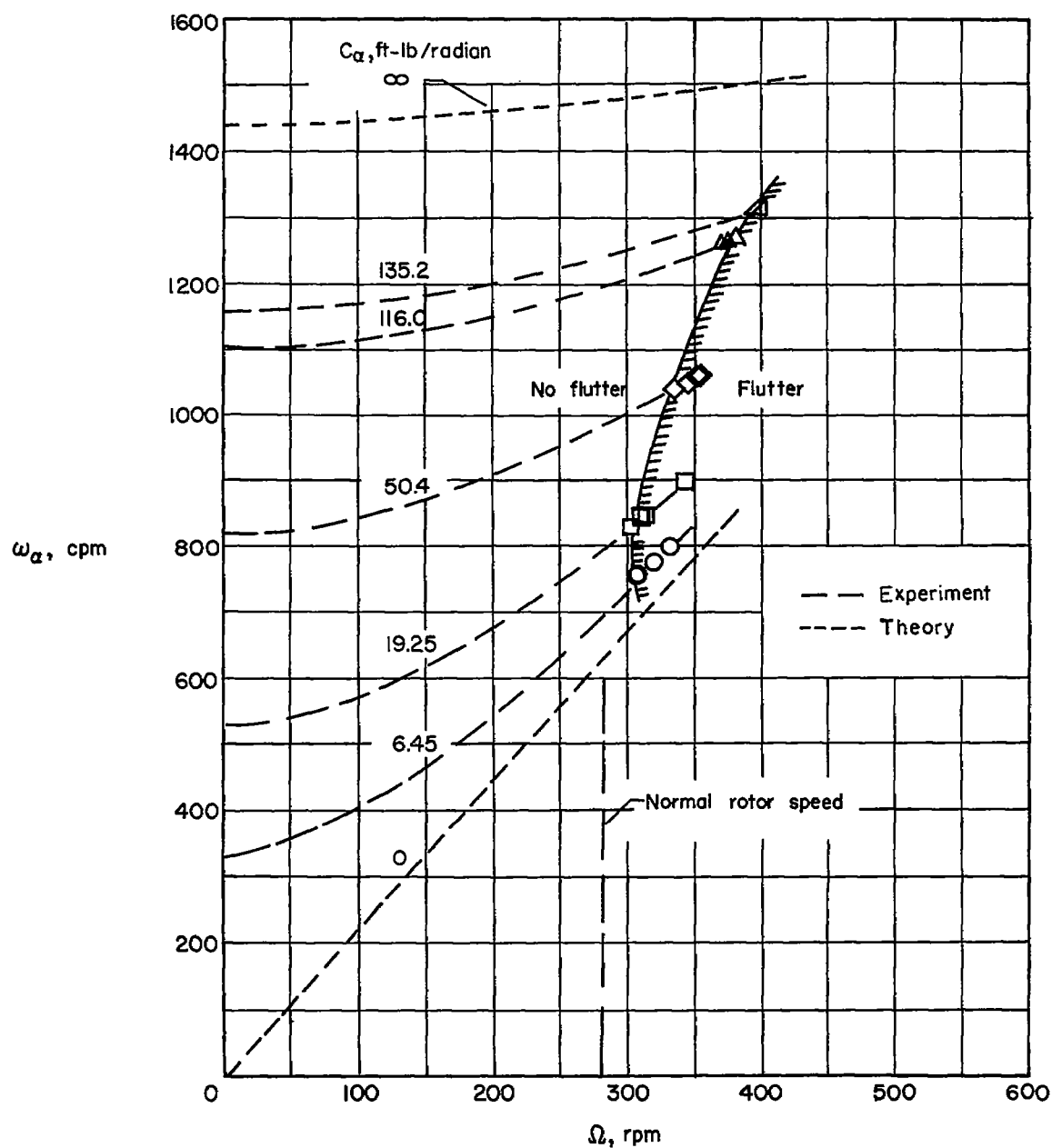


Figure 11.- Effect of torsional frequency on flutter speed.

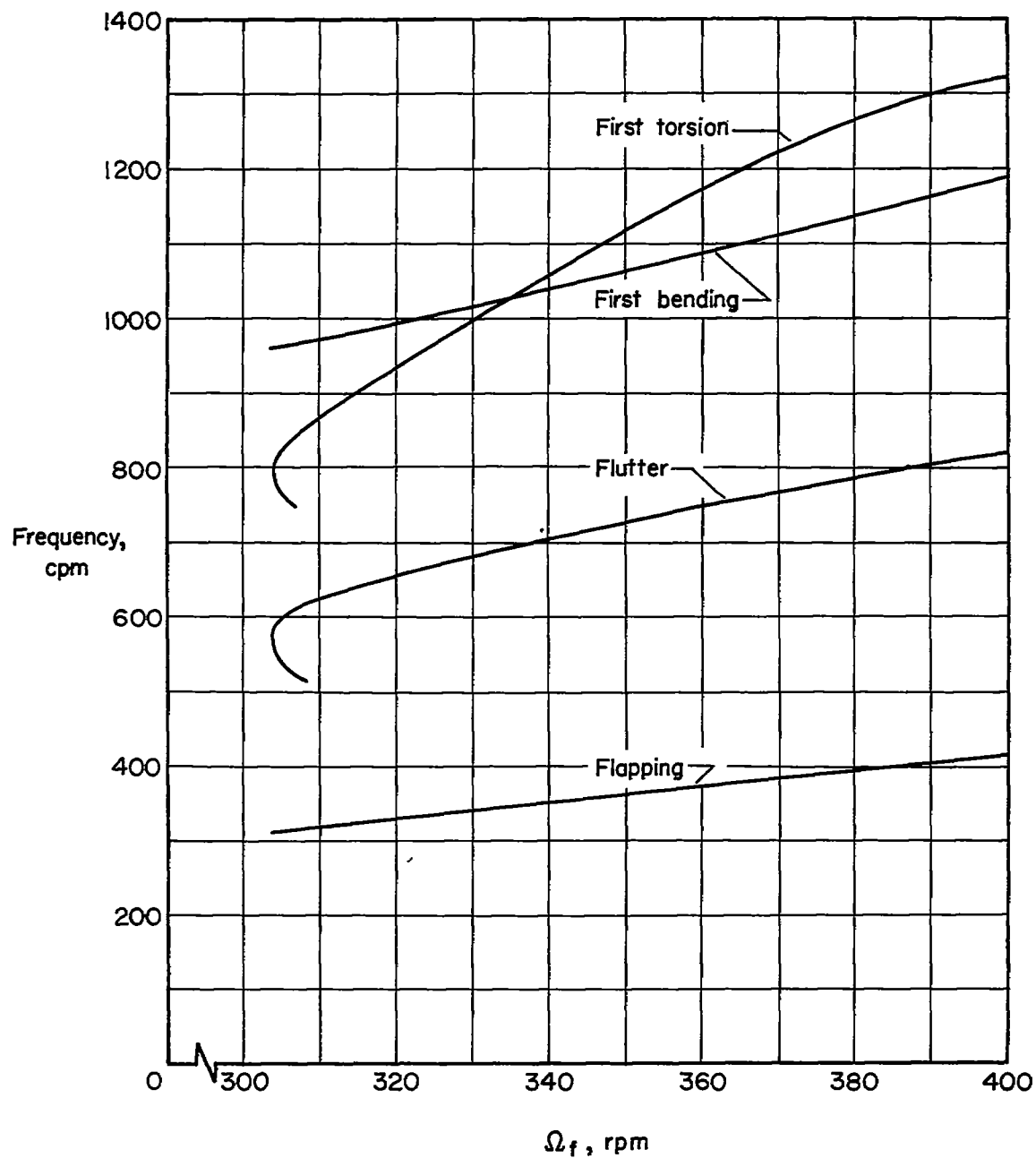
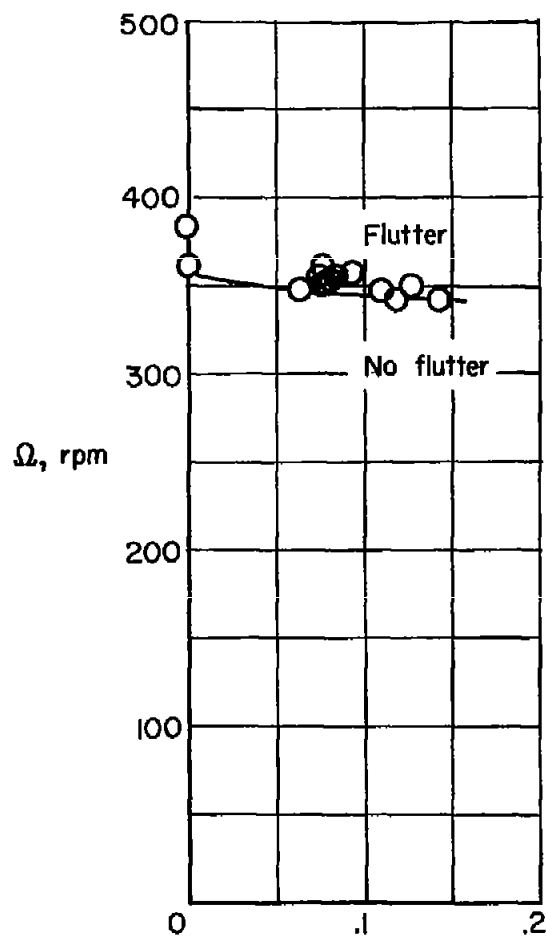
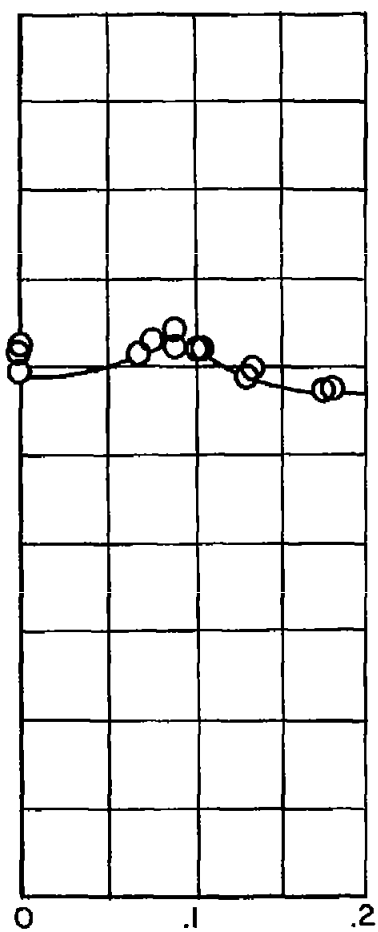


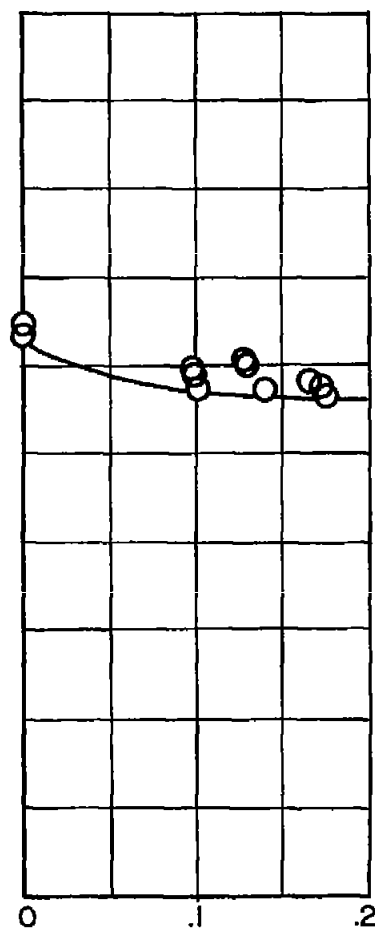
Figure 12.- Variation of significant blade frequencies with rotor speed at flutter.



(a) Blade configuration 6.



(b) Blade configuration 7.



(c) Blade configuration 8.

Figure 13.- Effect of tip-speed ratio on rotor rotational speed at flutter.

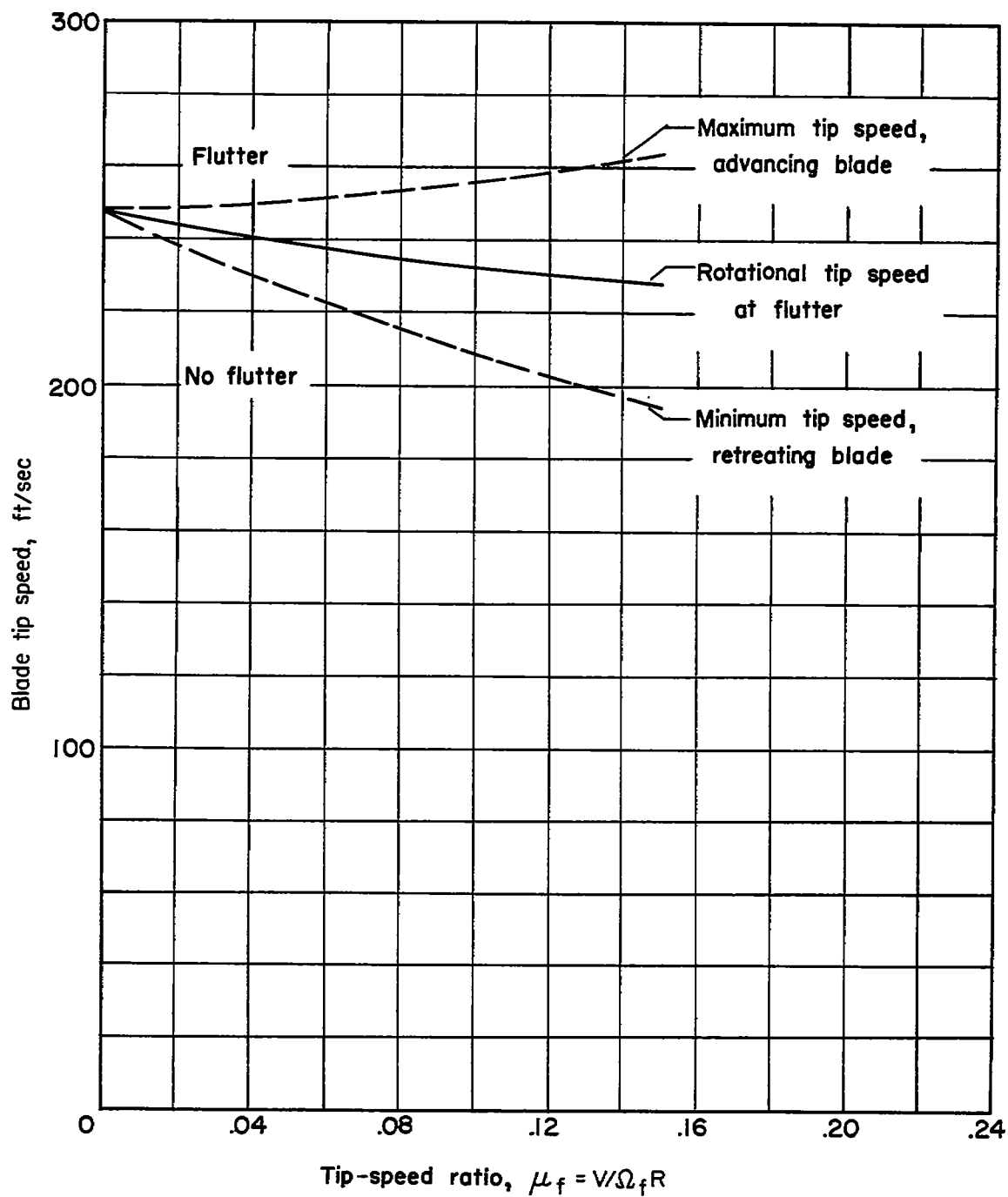


Figure 14.- Effect of tip-speed ratio on blade-tip speed at flutter.
Configuration 6.

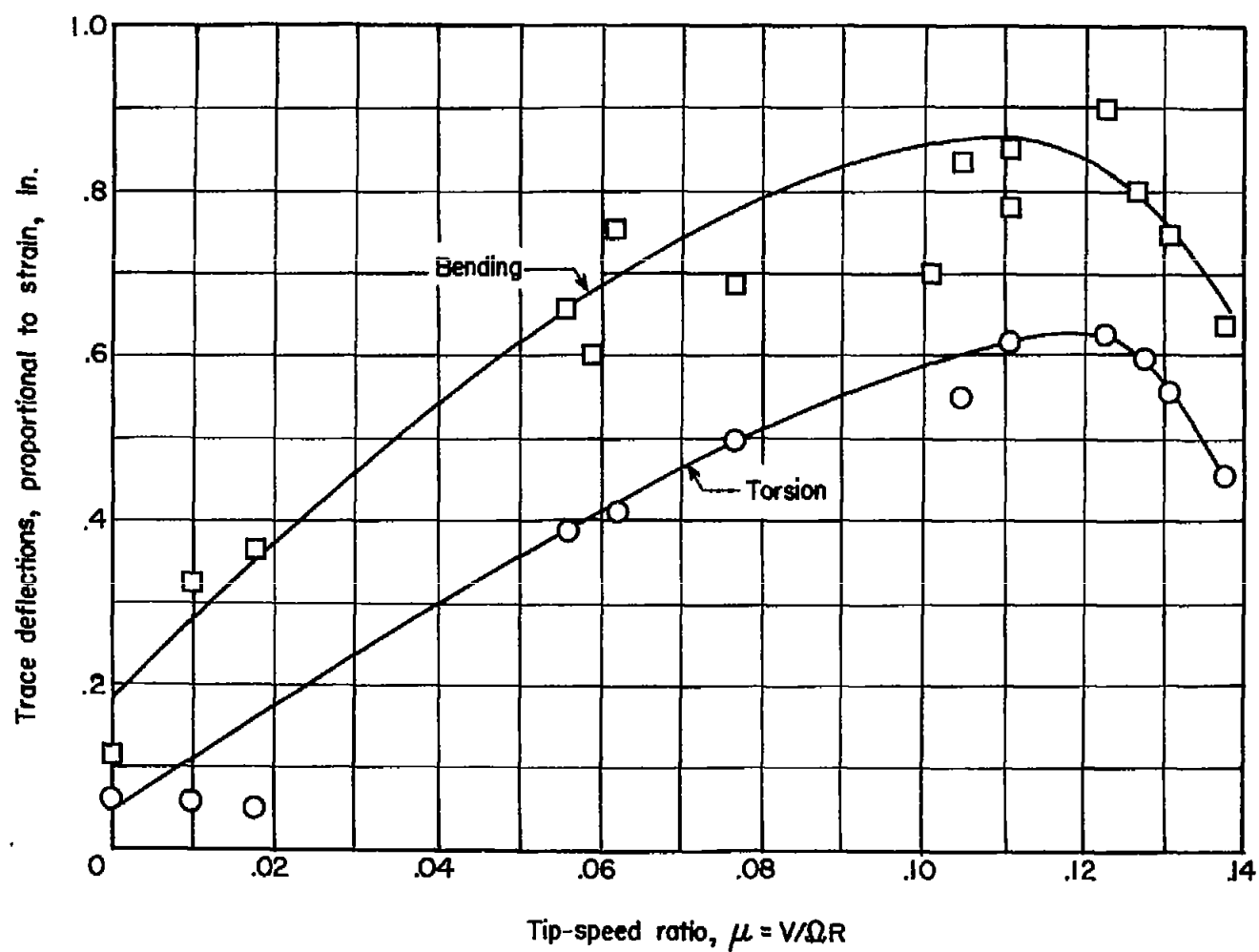


Figure 15.- Effect of tip-speed ratio on blade bending and torsion strain-gage response at normal rotor speed with inboard counterweight attached. Configuration 6.

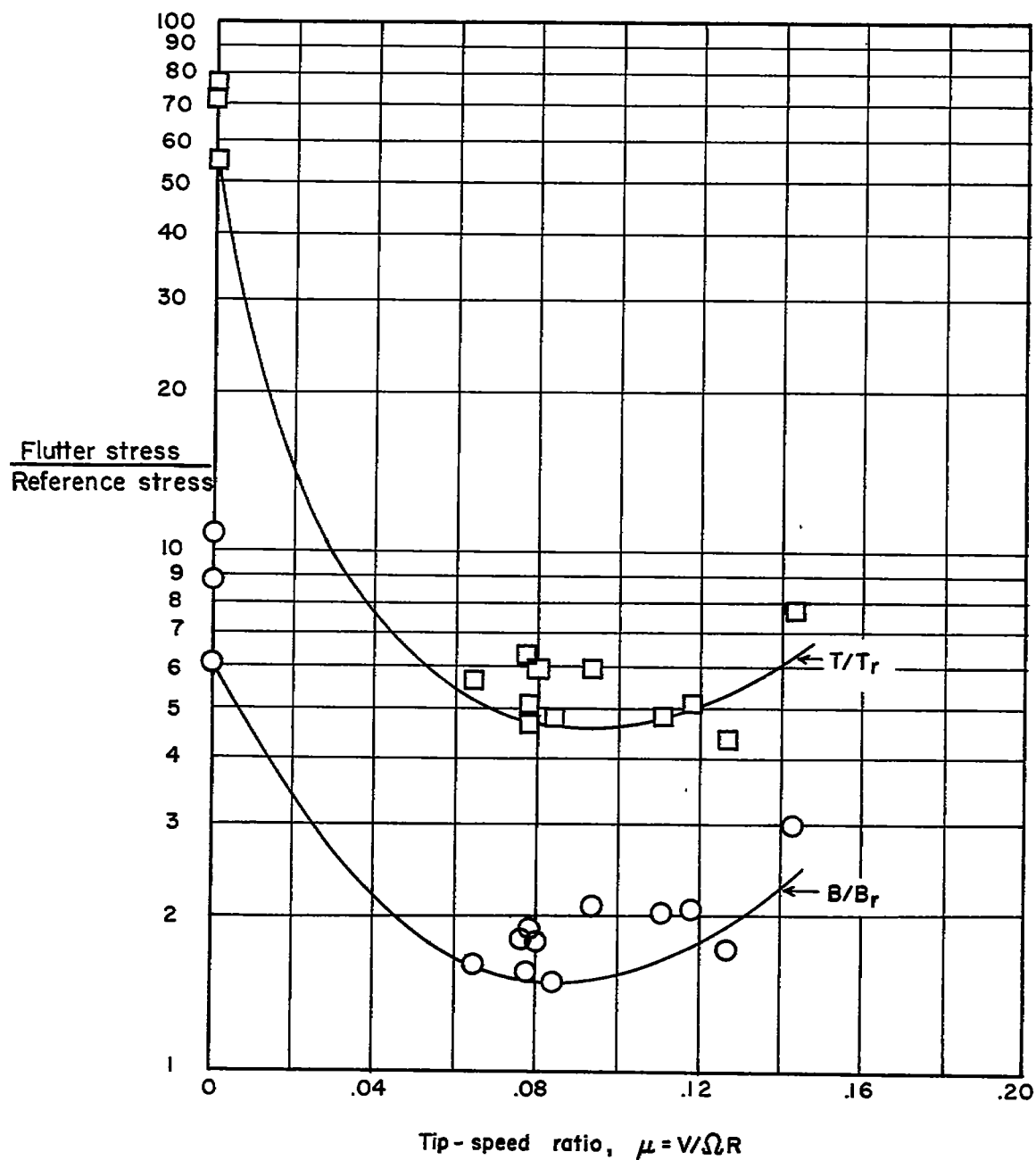


Figure 16.- Effect of tip-speed ratio on the ratio of the strain-gage response at flutter to the strain-gage response at normal operating speed. Configuration 6.

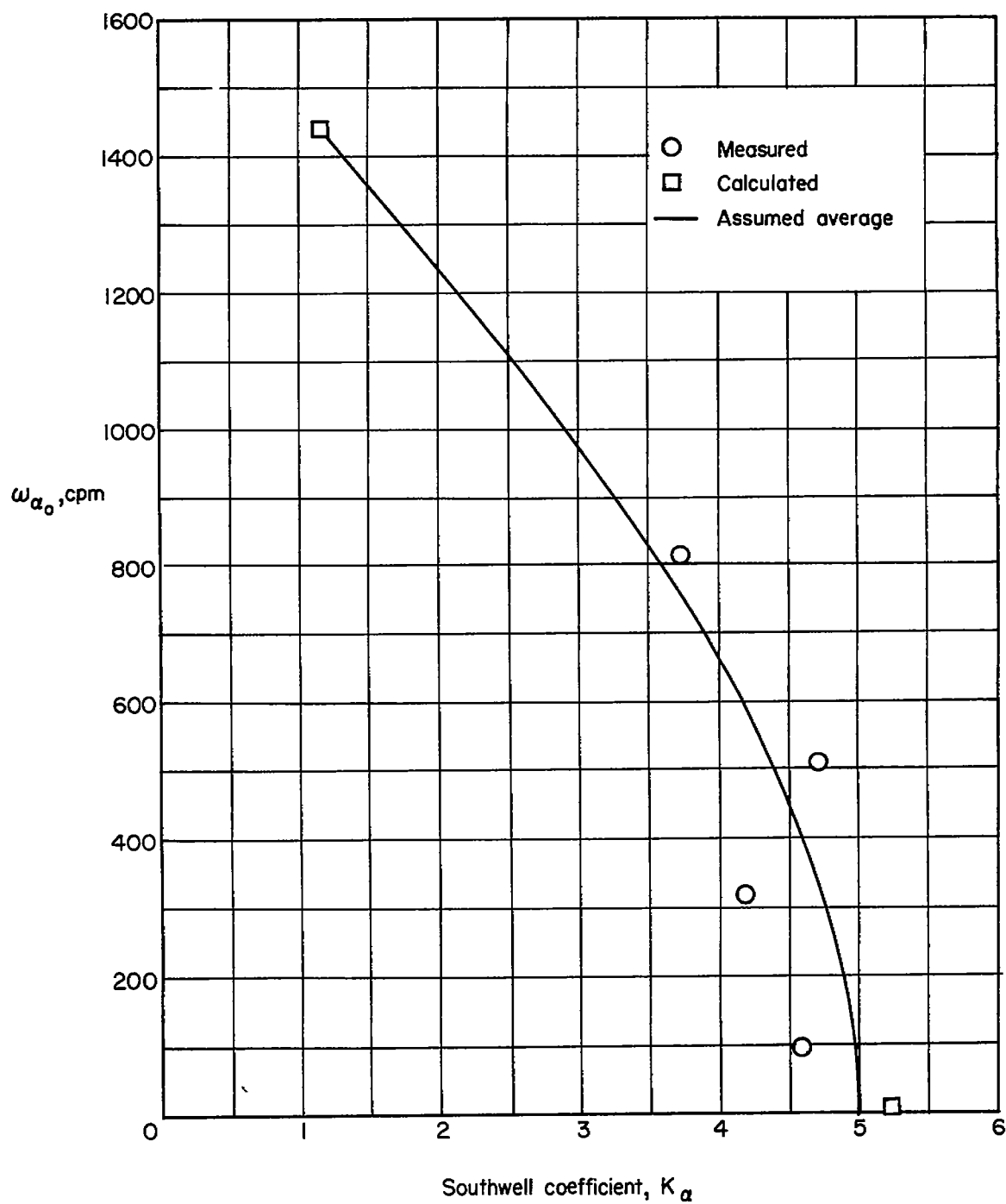


Figure 17.- Variation of Southwell coefficient for torsion with torsional frequency.

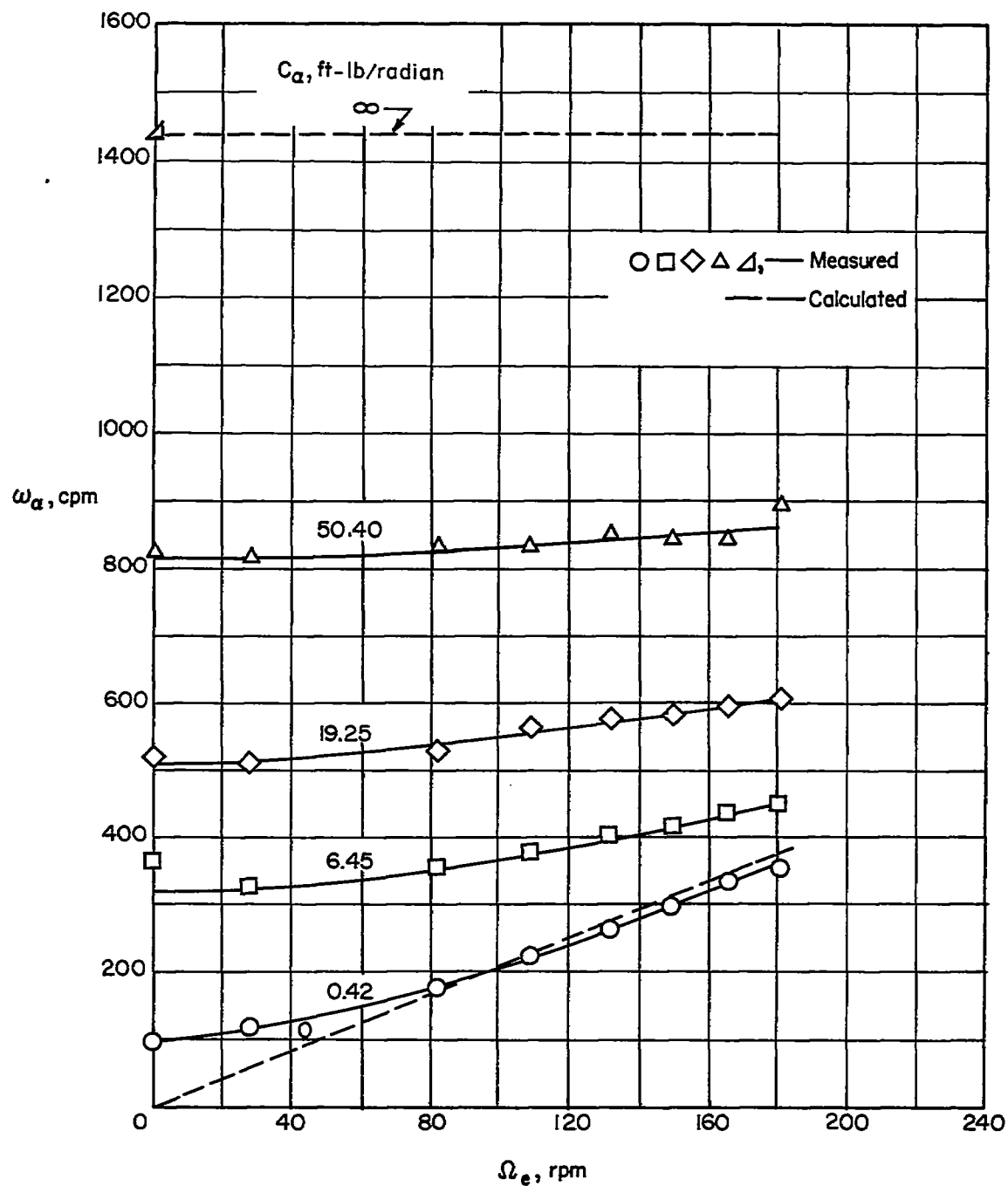


Figure 18.- Variation of torsional frequency with effective rotor speed.

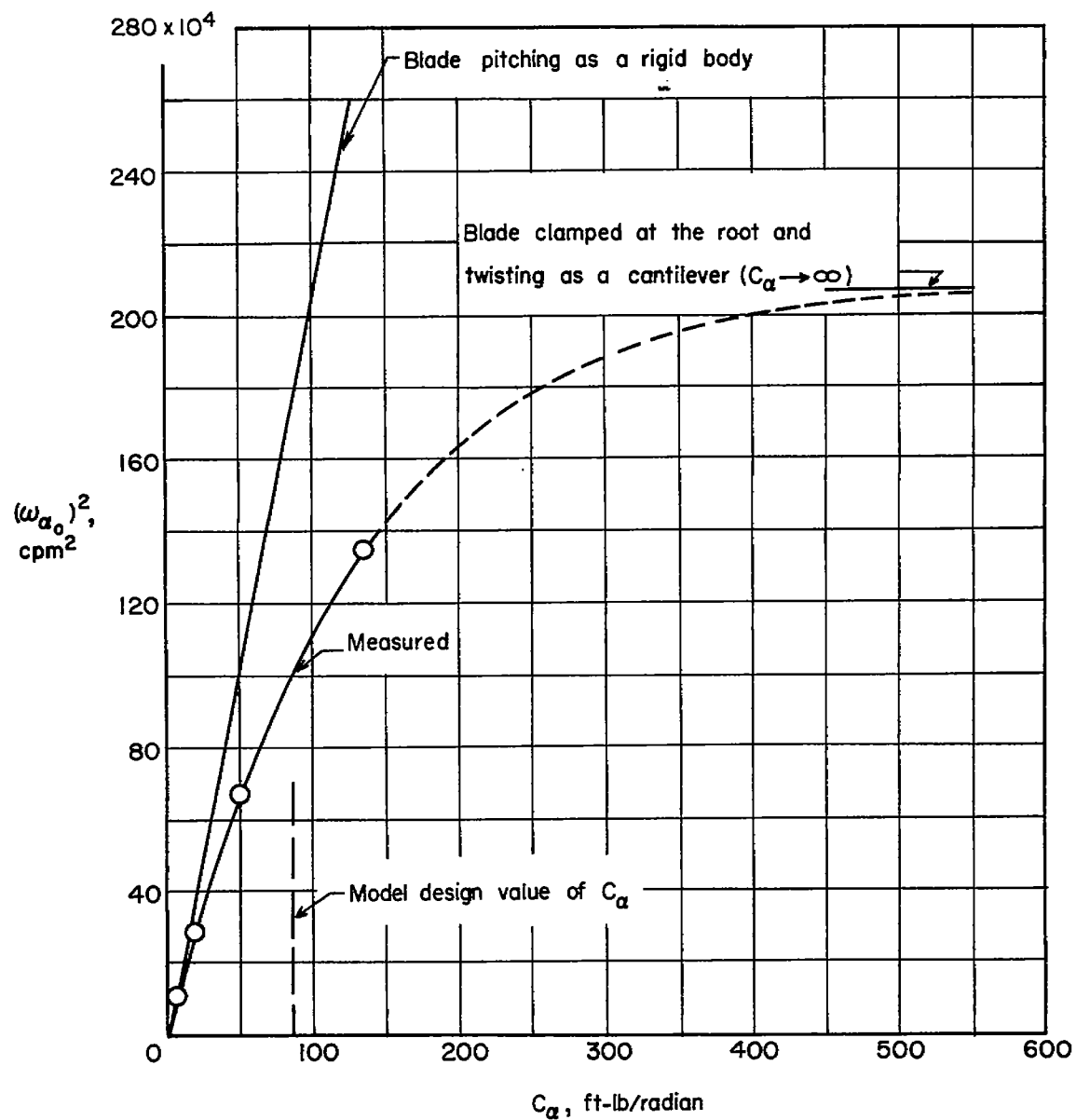


Figure 19.- Effect of control stiffness on torsional frequency.